# Microstructural Modification of As-Cast Al-Si-Mg Alloy by Friction Stir Processing

Z.Y. MA, S.R. SHARMA, and R.S. MISHRA

Friction stir processing (FSP) has been applied to cast aluminum alloy A356 plates to enhance the mechanical properties through microstructural refinement and homogenization. The effect of tool geometry and FSP parameters on resultant microstructure and mechanical properties was investigated. The FSP broke up and dispersed the coarse acicular Si particles creating a uniform distribution of Si particles in the aluminum matrix with significant microstructural refinement. Further, FSP healed the casting porosity. These microstructural changes led to a significant improvement in both strength and ductility. Higher tool rotation rate was the most effective parameter to refine coarse Si particles, heal the casting porosity, and consequently increase strength. The effect of tool geometry was complicated and no systematic trend was observed. For a standard pin design, maximum strength was achieved at a tool rotation rate of 900 rpm and traverse speed of 203 mm/min. Post-FSP aging increased strength for materials processed at higher tool rotation rates of 700 to 1100 rpm, but exerted only a marginal effect on samples prepared at the lower rotation rate of 300 rpm. Two-pass FSP with 100 pct overlapping passes resulted in higher strength for both as-FSP and post-FSP aged conditions.

## I. INTRODUCTION

THE Al-7 wt pct Si-Mg alloys with Mg contents in the range of 0.25 to 0.65 wt pct (A356 and A357 alloys) are widely used to cast high-strength components in the aerospace and automobile industries because they offer a combination of high strength[1,2,3] with good casting characteristics.[4] However, some mechanical properties of cast alloys, in particular, ductility, toughness, and fatigue resistance, are limited by three microstructural features: porosity, coarse acicular Si particles, and coarse primary aluminum dendrites.[5–8]

In the past two decades, various modification and heat-treatment techniques have been developed to refine the microstructure of cast Al-Si alloys. The first category of research is aimed at modifying the morphology of Si particles. Generally, chemical modification and thermal treatment have been adopted to modify the coarse acicular Si particles to fine and globular particles.[8,9,10] Chemical modification methods involve adding very small amounts of sodium, strontium, or antimony, known as eutectic modifiers.[9,10] Sodium is a good modifier and traditionally has been used to spheroidize eutectic particles. However, the benefits of sodium fade rapidly on holding at high temperature and the modifying action practically disappears after only two remelts. On the other hand, the modifying effect of strontium does not fade on holding at elevated temperature and its use has become more widespread. However, dissolution of strontium is difficult and a longer holding time is required at 750 °C, resulting in increased gas pickup.[11] Furthermore, the density of microshrinkage porosity is also higher after the addition of strontium owing to the dissolution difficulty and a depression in the eutectic transformation temperature.[12] Finally, although antimony has no fading effect and the improvement in elongation and impact strength is greater than that achieved by sodium,[9] environmental and safety concerns have precluded its use in most countries. Thermal modification involves heat treatment of cast alloys at high temperature, usually at the solid solution temperature around 540 °C for long times.[8] Solution heat treatment results in a substantial degree of spheroidization of Si particles and also coarsens Si particles. However, solution treatment at high temperature for long time increases material cost.

The second research category refines the coarse primary aluminum phases. Heat treatment at an extremely high temperature of 577 °C for a short time of 8 minutes resulted in a substantial refinement in the aluminum dendrites in a semisolid processed A356.[3] This heat treatment increases both yield and ultimate tensile strengths of A356.[3] More recently, Wang *et al.*[13] reported that a melt thermal treatment led to a remarkable refinement of the aluminum phase in A356, thereby resulting in a significant improvement in both strength and ductility.

None of the modification and heat-treatment techniques mentioned previously can eliminate the porosity effectively in A356 and redistribute the Si particles uniformly into the aluminum matrix. Therefore, a more effective modification technique is highly desirable for microstructural modification of cast A356 to enhance mechanical properties, in particular, ductility and fatigue. Friction stir processing (FSP), a development based on friction stir welding (FSW),[14,15] is a new solid-state processing technique for microstructural modification.[16,17] The basic concept of FSP is remarkably simple. A rotating tool with pin and shoulder is inserted into a single piece of material and traversed along the desired path to cover the region of interest. The FSP results in severe plastic deformation and extensive material

Z.Y. MA, Professor, formerly with the Department of Materials Science and Engineering, Center for Friction Stir Processing, University of Missouri, is with the Institute of Metal Research, Chinese Academy of Sciences, Shenyang 110016, People's Republic of China. S.R. SHARMA, formerly with the Department of Materials Science and Engineering, Center for Friction Stir Processing, University of Missouri, is with Intel Corporation, Portland, OR 97124. R.S. MISHRA, Professor, is with the Department of Materials Science and Engineering, Center for Friction Stir Processing, University of Missouri, Rolla, MO 65409. Contact e-mail: rsmishra@umr.edu

Manuscript submitted January 8, 2006.

mixing in the processed zone and thus modifies the local microstructure. The characteristics of FSP have resulted in several applications for microstructural modification in metallic materials, including high strain rate superplasticity,[16–20] surface composite,[21] and homogenization of nanophase aluminum alloys and aluminum matrix composites.[22,23]

In a previous study, we reported preliminary results of the microstructural modification of sand-cast A356 *via* FSP.[24] It was shown that FSP broke up and dispersed coarse acicular Si particles, resulting in significantly enhanced mechanical properties.[24,25] In this study, the effect of FSP on microstructure and properties of sand-cast A356 was evaluated in detail, including (a) thermal profiles during FSP, (b) effect of heat treatment on microstructure and properties of FSP samples, (c) mechanical properties of microstructural transition regions, and (d) fracture characteristics of FSP samples.

## II. EXPERIMENTAL

Commercial A356 sand-cast plates with composition of 7.20Si-0.36Mg-0.13Fe-0.16Ti-0.014Cu-0.018Zn-0.007Mn-0.003Cr-0.007Ni-bal Al (in wt pct) were used for FSP. The plates with the same dimensions (16-mm thick) were received in the as-cast condition. All the plates were cast with the same cast technology and, therefore, exhibited similar microstructural characteristics. All FSP runs were performed on a single plate along the centerline of the A356 cast plate to assure similar starting microstructure. Pin geometries and processing parameters used for FSP are summarized in Table I. Figure 1 shows the geometry of various pins used for FSP. Thermal profiles during FSP were recorded by embedding a thermocouple in the regions adjacent to the rotating pin. For these FSP runs, the thermocouples were embedded at the same locations (5 mm from the weld centerline, 5 mm from the top surface of the plate, and 150 mm from the FSP start point) to acquire accurate and comparable temperature profiles. As-processed aluminum plates were cut transverse to the processing direction, mounted, and mechanically polished. Microstructural examination was completed with optical microscopy (OM), scanning electron microscopy (SEM, JEOL* T330A), and transmission electron microscopy (TEM, PHILIPS** EM430). Thin foils for TEM were prepared by ion thinning and jet polishing techniques, respectively. Jet polishing was conducted at −25 °C using a solution of 20 pct $HNO_3$ + 80 pct methanol (in volume). The size and aspect ratio of Si particles and the porosity level were analyzed using Scion Image software. An equivalent diameter, $D$ ($D = (d_L d_T)^{1/2}$), was used to define the size of Si particles, where $d_L$ and $d_T$ are the dimensions of the major and minor axes of the particles, respectively. The aspect ratio of Si particles is defined as the ratio of $d_L$ and $d_T$.

**Table I. Summary of Pin Geometry and Processing Parameters for FSP A356**

| Processing Parameter | Tool Geometry | | |
|---|---|---|---|
| | Standard Pin (S-Pin) | Tri-flute Pin (T-Pin) | Cone-Shaped Pin (C-Pin) |
| 300 rpm–51 mm/min | x | x | x |
| 700 rpm–203 mm/min | x | x | x |
| 900 rpm–203 mm/min | x | x | — |
| 1100 rpm–203 mm/min | x | x | — |

Following FSP, samples were kept at room temperature for more than one month to naturally age to stabilize the microstructure. Mini-tensile specimens of 1.3-mm gage length and 1.0-mm gage width were electrodischarge machined transverse to the FSP direction with the gage center being at the center of the FSP region. These specimens were subsequently ground and polished to a final thickness of ~0.5 mm. Tensile tests were conducted at room temperature using a computer-controlled, custom-built mini-tensile tester with an initial strain rate of $1 \times 10^{-3}$ $s^{-1}$. The property data for each condition were obtained by averaging five test results. For comparison, mini specimens of the as-received A356 were also tested

*JEOL is a trademark of Japan Electron Optics Ltd., Tokyo.

**PHILIPS is a trademark of Philips Electronic Instruments Corp., Mahwah, NJ.

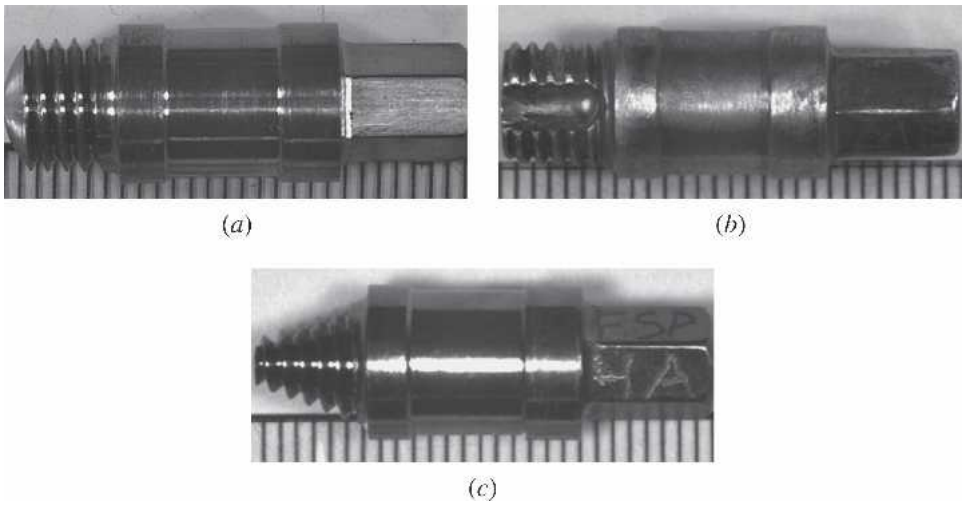


Fig. 1—Pins used for FSP: (*a*) standard pin, (*b*) triflute pin, and (*c*) cone-shaped pin.

using the same experimental conditions and specimen geometry. To understand the effect of heat treatment on post-FSP properties, samples were subjected to artificial aging (155 °C for 4 hours) and T6 temper (solutionized at 540 °C/4 h, water quenched, and aged at 155 °C/4 h). To measure the mechanical properties of microstructural transition regions in FSP samples, mini-tensile specimens were machined from various locations, *i.e.,* at different distances from the FSP centerline. The fracture surfaces of tensile specimens were examined using SEM. Further, longitudinal cross sections of failed specimens were mounted, mechanically polished, and observed by OM.

## III. RESULTS

### A. *Thermal Exposure during FSP*

Figure 2 shows a typical thermal profile for FSP of A356 at a tool rotation rate of 900 rpm and a traverse speed of 203 mm/min (hereafter referred to as 900 rpm–203 mm/min) by triflute pin. A peak temperature of 478 °C was recorded. It is noted from Figure 2 that both heating and cooling rates are quite rapid. The duration at above 200 °C is only 25 seconds. Table II shows peak temperatures recorded for FSP A356 at various FSP parameters by triflute pin. Generally, peak temperature increases with increasing tool rotation rate. However, a decrease in peak temperature was observed at a higher tool rotation rate of 1100 rpm.

### B. *Microstructure*

Figure 3 shows optical micrographs of a polished A356 casting in the as-cast condition. Coarse acicular Si particles were distributed along the primary aluminum dendrite boundaries. The average dendrite size was 100 to 200 $\mu$m and the Si particles had lengths of up to 100 $\mu$m. Furthermore, porosity of up to 100 $\mu$m in diameter (not shown) was detected in the as-received A356 plates.

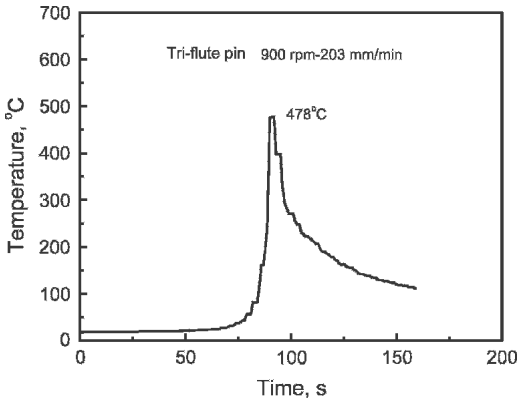


Fig. 2—Thermal profile for FSP of A356 at 900 rpm–203 mm/min by triflute pin.

**Table II. Peak Temperature (°C) Measured in FSP of A356 Plates Using Tri-Flute Pin**

| | Traverse, Speed, mm/min | |
|---|---|---|
| Rotation Rate, rpm | 51 | 203 |
| 300 | 407 | — |
| 700 | — | 452 |
| 900 | — | 478 |
| 1100 | — | 461 |

Figure 4 shows optical micrographs of FSP A356 samples for various processing parameters using the triflute pin. The FSP resulted in a significant breakup of acicular Si particles and aluminum dendrites, and subsequently created a uniform distribution of smaller broken Si particles in the aluminum matrix. The size and aspect ratio of Si particles in the FSP A356 decrease with increasing tool rotation rate (Figures 4(a) through (c)). In addition, two-pass FSP, with 100 pct overlapping, results in an increase in the number of small-sized Si particles (compare Figures 4(c) and (d)). Furthermore, FSP nearly eliminated porosity in the as-cast A356. Similar trends were observed in samples processed using standard pin (Figure 5) and cone-shaped pin designs, namely, higher tool rotation rates resulted in smaller Si particle sizes and aspect ratios.

The size and aspect ratio of Si particles and porosity level in both as-cast and FSP A356 samples are summarized in Table III. Figure 6 shows the distribution of Si particle size in as-cast A356 and FSP A356 samples. Table IV shows the distribution statistics of Si particle size in the FSP A356 samples. Because the Si particles frequently connect to each other in the as-cast alloy, this tends to overestimate the particle size and underestimate their aspect ratio by means of Scion Image software. Therefore, the computerized calculation of size and aspect ratio of Si particles for the as-cast alloy is subject to error. To eliminate this error, manual measurements were used for the as-cast alloy. Four important observations can be made from Tables III and IV and Figure 6. First, FSP resulted in significant decreases in the size and aspect ratio of Si particles and the porosity level. The broken Si particles have a size ranging from submicron to more than ten micrometer, resulting in a large standard deviation of measured Si particle size, as listed in Table III. Second, increasing the tool rotation rate from 300 to 700 to 1100 rpm resulted in a further reduction in both the size and aspect ratio of Si particles and porosity level. Such a decrease in the Si particle size is due to the increase in quantity of smaller particles and the decrease in quantity of larger particles (Table IV). Third, at a constant traverse speed of 203 mm/min, generally, the Si particle size decreased with increasing tool rotation rate from 700 to 1100 rpm. However, the aspect ratio of Si particles and the porosity level did not show a consistent trend with increasing tool rotation rate. Fourth, two-pass FSP with 100 pct overlapping passes did not result in a significant decrease in the Si particle size, but increased the number of small-sized Si particles. The fraction of Si particles of smaller than 1.5 $\mu$m increased from 39 pct for single-pass FSP to 42 pct for two-pass FSP.

Compared to the as-cast A356 sample, the edges or corners of Si particles in the T6-treated cast sample become rounded. However, T6 treatment did not result in appreciable fragmentation and spheroidization of coarse acicular Si particles. On the other hand, T6 treatment led to spheroidization of the broken Si particles to a certain extent in FSP A356 samples (compare Figures 4(a) and (b) and 7(a) and (b)). For example, the aspect ratio of Si particles in FSP A356 samples prepared at 300 rpm–51 mm/min and

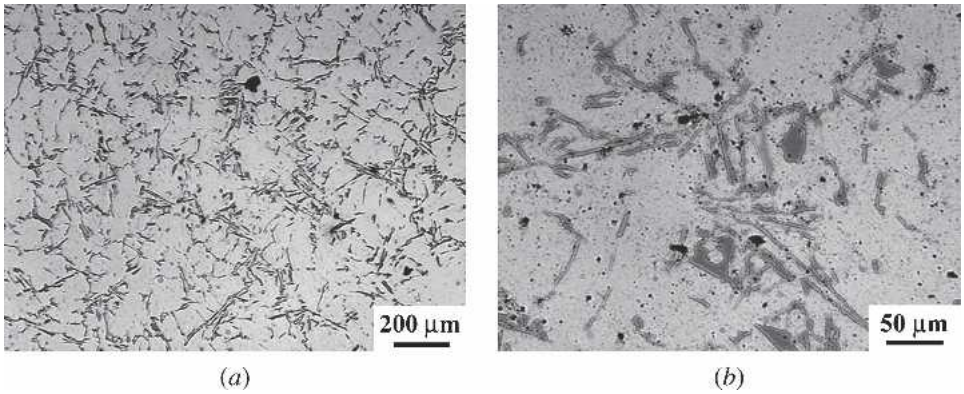


Fig. 3—Optical micrographs showing the dendritic structure and morphology of Si particles in as-cast A356.

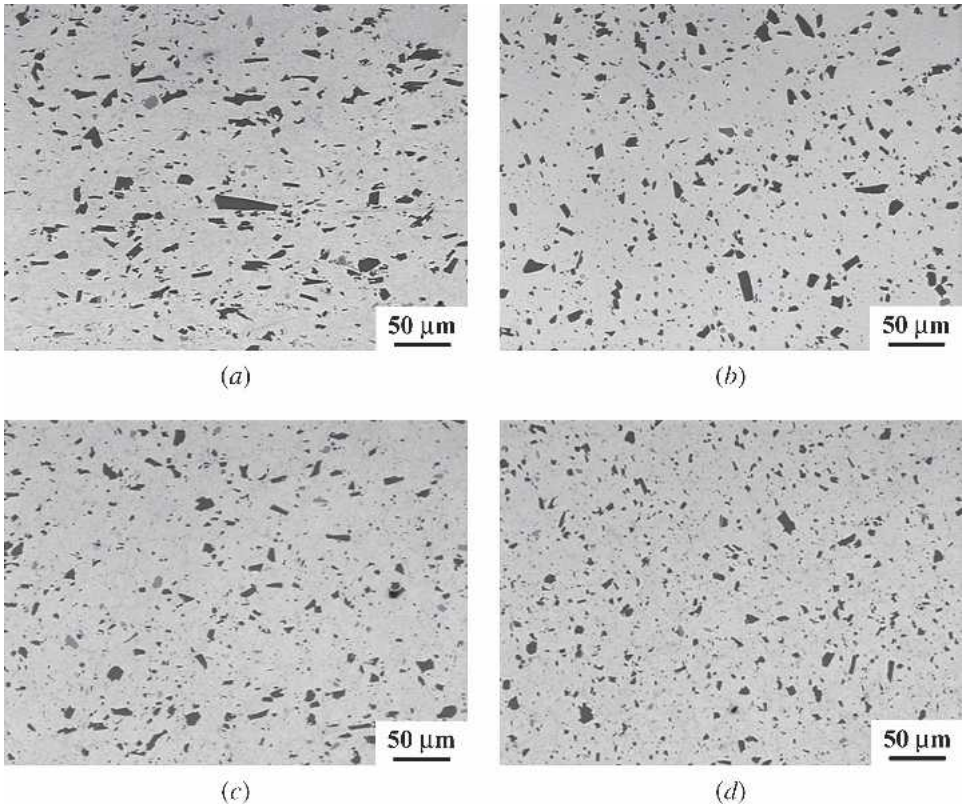


Fig. 4—Optical micrographs showing morphology and distribution of Si particles in FSP A356 samples prepared using a triflute pin at (*a*) 300 rpm–51 mm/min, (*b*) 700 rpm–203 mm/min, (*c*) 900 rpm–203 mm/min, and (*d*) 900 rpm–203 mm/min (two pass with 100 pct overlapping).

700 rpm–203 mm/min decreased from 2.30 and 1.94 in the as-FSP condition to 1.93 and 1.59 following FSP + T6 (Table III). Although Figures 7(a) and (b) did not show substantial coarsening of Si particles, the fine Si particles in the as-FSP condition disappeared after the T6 treatment. Table IV demonstrates that T6 treatment resulted in a significant reduction in the quantity of smaller Si particles and an obvious increase in the quantity of larger Si particles. This resulted in an increase in average Si particle size. The average Si particle size in FSP A356 samples prepared at 300 rpm–51 mm/min and 700 rpm–203 mm/min increased from 2.70 and 2.50 in the as-FSP condition to 3.69 and 3.05 following the T6 heat treatment.

Figure 8 shows TEM micrographs of as-cast and FSP A356 samples. In the as-cast A356 sample, coarse needlelike $Mg_2Si$ phases were distinctly discernible and there is very low dislocation density (Figure 8(a)). In the FSP A356 samples, no coarse needlelike $Mg_2Si$ phases were observed (Figures 8(b) through (d)) and the grains were ~5 to 8 $\mu$m (Figure 8(b)) and refined significantly. Numerous homogeneously distributed fine particles were observed in the aluminum matrix (Figure 8(b)). These fine particles exhibited irregular shapes (Figure 8(c)) and were identified to be Si phase by electron diffraction pattern. Furthermore, high dislocation density was observed in the FSP A356 samples and the interaction between fine Si particles and dislocations was often observed (Figure 8(d)).

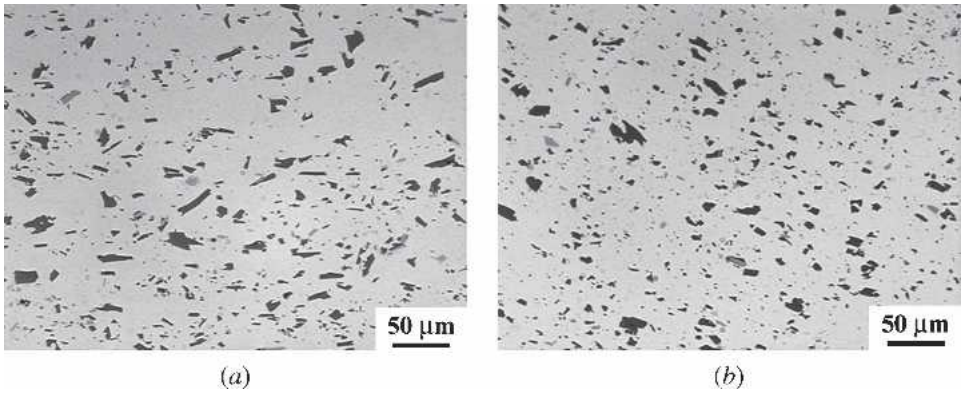


Fig. 5—Optical micrographs showing morphology and distribution of Si particles in FSP A356 samples prepared using the standard pin at (*a*) 300 rpm–51 mm/min and (*b*) 900 rpm–203 mm/min.

**Table III. Size and Aspect Ratio of Si Particles and Porosity Volume Fraction in FSP and As-Cast A356**

| Material | Particle Size ($\mu$m) | Aspect Ratio | Porosity Volume Fraction (Pct) |
|---|---|---|---|
| As cast | 16.75 ± 9.21 | 5.92 ± 4.34 | 0.95 |
| FSP, 300 rpm–51 mm/min (S-pin) | 2.84 ± 2.37 | 2.41 ± 1.33 | 0.11 |
| FSP, 700 rpm–203 mm/min (S-pin) | 2.62 ± 2.31 | 1.93 ± 0.86 | 0.050 |
| FSP, 900 rpm–203 mm/min (S-pin) | 2.55 ± 2.21 | 2.00 ± 1.01 | 0.027 |
| FSP, 1100 rpm–203 mm/min (S-pin) | 2.51 ± 2.00 | 2.04 ± 0.91 | 0.042 |
| FSP, 300 rpm–51 mm/min (T-pin) | 2.70 ± 2.26 | 2.30 ± 1.15 | 0.087 |
| FSP, 300 rpm–51 mm/min (T-pin)-T6 | 3.69 ± 2.55 | 1.93 ± 0.90 | — |
| FSP, 700 rpm–203 mm/min (T-pin) | 2.50 ± 2.02 | 1.94 ± 0.88 | 0.024 |
| FSP, 700 rpm–203 mm/min (T-pin)-T6 | 3.05 ± 2.04 | 1.59 ± 0.55 | — |
| FSP, 900 rpm–203 mm/min (T-pin) | 2.50 ± 2.04 | 1.99 ± 0.94 | 0.032 |
| FSP, 900 rpm–203 mm/min (T-pin)-2 pass | 2.43 ± 2.02 | 1.86 ± 0.78 | 0.020 |
| FSP, 1100 rpm–203 mm/min (T-pin) | 2.44 ± 2.00 | 1.86 ± 0.81 | 0.025 |
| FSP, 300 rpm–51 mm/min (C-pin) | 2.90 ± 2.46 | 2.50 ± 1.35 | 0.094 |
| FSP, 700 rpm–203 mm/min (C-pin) | 2.86 ± 2.32 | 2.09 ± 0.90 | 0.032 |

S: standard, T: tri-flute, and C: cone shaped.

### C. *Tensile Properties*

Table V summarizes the room-temperature tensile properties of as-cast and FSP A356 samples under as-FSP and aged conditions. The as-received A356 cast plate exhibited an ultimate tensile strength of 169 MPa, a yield strength of 132 MPa, and an elongation of 3 pct. The FSP resulted in a significant improvement in tensile properties, particularly the ductility. The elongation to failure increased by one order of magnitude after FSP.

Experimental data for the as-FSP condition in Table V revealed four important observations. First, FSP at higher tool rotation rates (700 to 1100 rpm) resulted in higher strength than that at the lower rotation rate of 300 rpm. Second, FSP samples prepared using the triflute pin at higher tool rotation rates of 900 and 1100 rpm exhibited better ductility. Third, at a constant tool traverse speed of 203 mm/min, maximum strength was observed at 900 rpm for the standard pin, whereas a minimum strength was obtained at 900 rpm for the triflute pin. Fourth, two-pass FSP resulted in higher yield and ultimate tensile strengths compared to one-pass FSP.

The property data following aging (155 °C for 4 hours) provides additional observations. First, the aging treatment of as-cast A356 resulted in a slight increase in yield strength, but a decrease in ultimate tensile strength and ductility. Second, at the lower rotation rate of 300 rpm, the aging treatment had little effect on the mechanical properties of FSP A356 samples. For the standard and cone-shaped pins, the aging treatment at 300 rpm did not change the strength and ductility. For the triflute pin, at 300 rpm, the aging treatment increased the strength slightly and decreased the ductility. Third, at higher tool rotation rates of 700 to 1100 rpm, the aging treatment resulted in an increase in strength, particularly the yield strength of FSP A356 and some decrease in ductility. Fourth, the aged two-pass FSP sample prepared by the triflute pin at 900 rpm–203 mm/min exhibited the highest ultimate tensile strength of 304 MPa and yield strength of 236 MPa among all the FSP samples.

Tensile properties of T6-treated cast and FSP A356 samples are summarized in Table VI. The following observations can be made. First, the T6 treatment resulted in an increase in the strength of both cast and FSP A356 samples and a reduction in the ductility (compare Tables V and VI). Second, the T6 ultimate tensile strength and ductility of FSP samples are significantly superior to those of the cast alloy aged to T6. However, both the cast and FSP samples exhibited similar yield strengths. Third, FSP T6 samples prepared at various processing parameters showed similar strengths and ductility except at 300 rpm–51 mm/min where a higher yield strength and a lower ductility were

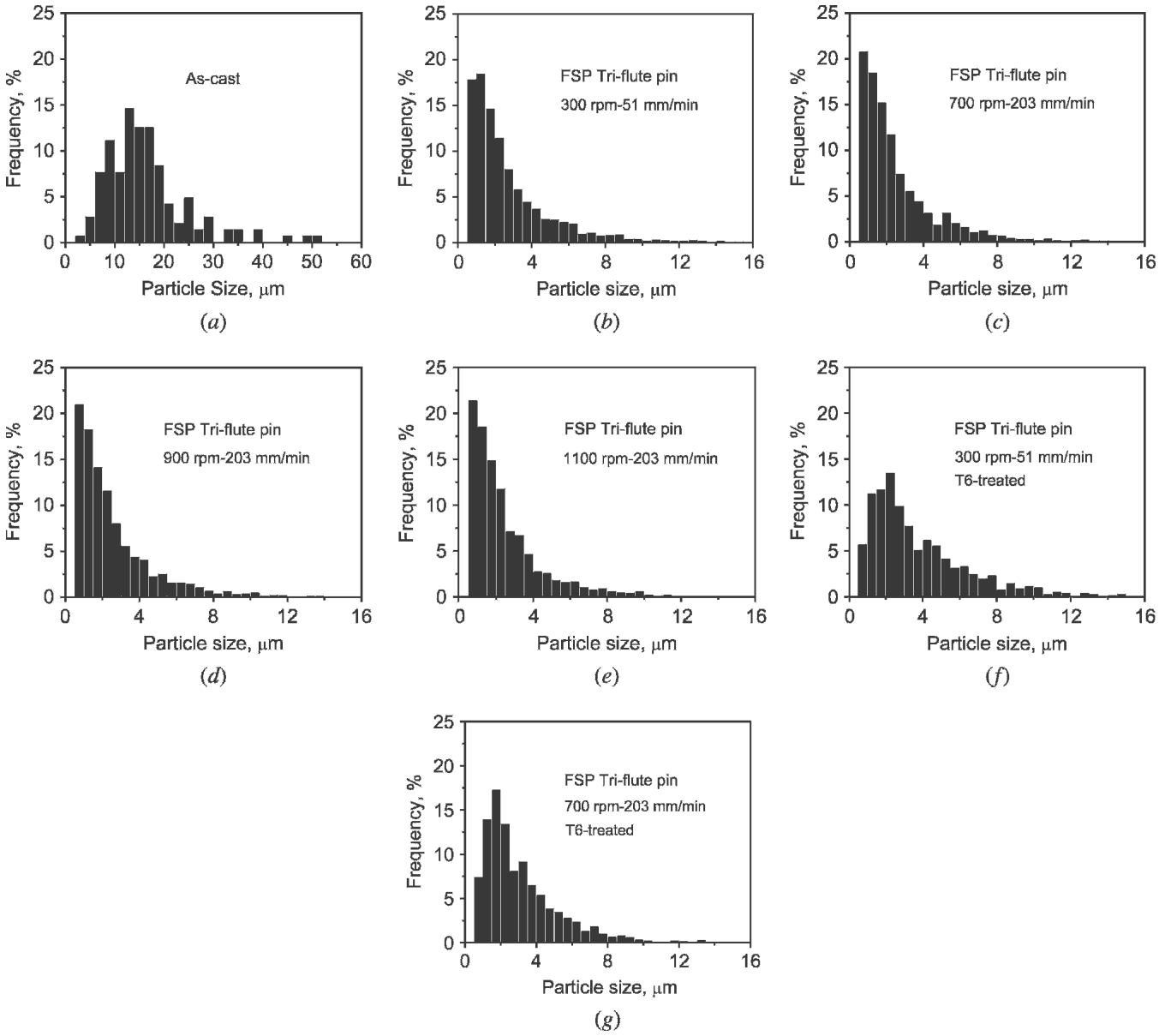


Fig. 6—Distribution of Si particle size in A356 samples under (*a*) as-cast; (*b*) FSP, 300 rpm–51 mm/min; (*c*) FSP, 700 rpm–203 mm/min; (*d*) FSP, 900 rpm–203 mm/min; (*e*) FSP, 1100 rpm–203 mm/min; (*f*) FSP–T6, 300 rpm–51 mm/min; and (*g*) FSP-T6, 700 rpm–203 mm/min (triflute pin).

observed. Fourth, there was no increase in either strength or ductility for the two-pass, FSP T6 sample compared to the one-pass FSP (Tables IV and V). In fact, data for both strength and ductility of the two-pass FSP sample showed the largest standard deviation.

Figure 9 shows tensile properties for the microstructural transition regions of FSP A356 samples. The strength and ductility of microstructural transition regions are equivalent to or lower than those of the parent metal. Both tensile and yield strengths of the microstructural transition regions decrease with increasing distance from the nugget zone.

### D. *Fracture Behavior*

Figure 10 shows polished cross-sectional views of failed tensile specimens of both cast and FSP A356. As-cast A356 samples showed low strain ductile failure without necking. Crack propagated mainly through the fracture or cleavage of Si particles (Figure 10(b)). As-FSP A356 samples showed necking (Figures 10(c) and (e)). No preferential crack propagation path was observed in the FSP samples (Figures 10(d) and (f)). However, fracture of some larger Si particles was often observed at or near the fracture tip. Similar observations were also made for the T6-treated A356 samples, both as-cast and FSP.

Figure 11 shows a side view of failed A356 specimens machined from microstructural transition regions. In the transition regions between the nugget zone and parent metal, the Si particles cracked due to FSP tended to align along the flow line, *i.e.,* vertical to the tensile axis, and crack propagation was associated with Si particle fracture or cleavage (Figures 11(a) and (b)). In regions 1 and 5 mm

from the nugget boundaries, the microstructure is basically similar to that of the as-cast sample. Therefore, crack propagation occurred in a way similar to that in the cast alloy (Figures 11 (c) and (d)).

Figure 12 shows SEM micrographs of the fracture surfaces of failed A356 specimens. For the as-cast A356 sample, the fracture surface was characterized by fractured or cleaved coarse Si particles and showed features of a typical low strain ductile failure (Figure 12(a)). The fracture surface of the T6-treated A356 sample was similar to that of the as-cast A356 sample. The fracture surfaces of the as-FSP A356 samples exhibited ductile dimple fracture with a few fractured Si particles detected in some large dimples (Figure 12(b)). The fracture surfaces of T6-treated FSP A356 samples showed fewer and smaller dimples (Figure 12(c)).

## IV. DISCUSSION

### A. *Thermal Exposure during FSP*

It is important to obtain the information on the thermal profile during FSW and FSP to understand the microstructural evolution in such a process. Therefore, the temperature distribution during FSW and FSP was widely studied by various investigators. The peak temperatures, recorded by embedding thermocouple in the regions adjacent to the rotating pin, were generally reported to be in the range of 400 °C to 500 °C.[26–29] Figure 2 and Table II indicate that the peak temperatures recorded for FSP of A356 samples are within 400 °C to 480 °C and in good agreement with those reported in FSW aluminum alloys by other investigators. It is important to point out that the maximum temperature during FSP should be higher than the peak temperature recorded by the thermocouple because the thermocouple was actually located out of the region stirred by the rotating pin.

Figure 2 indicates that both heating and cooling rates are very rapid and the duration for the FSP region above 200 °C is only 25 seconds (3 seconds for heating to 478 °C and 22 seconds for cooling to 200 °C). This is attributed to localized intense friction and deformation and quick thermal dissipation due to the excellent thermal conductivity of aluminum alloy.

The peak temperatures during FSW and FSP are generally believed to increase with the increasing tool rotation rate due to increased deformation rate.[29,30,31] For the current study, the peak temperatures increased with the increasing tool rotation rate from 300 to 900 rpm. This is consistent with the reports by other investigators. However, increasing the tool rotation rate from 900 to 1100 rpm resulted in a decrease in the peak temperature of the FSP samples. The reason for this is not clear. A possible reason is reduced friction at a higher rotation rate due to increased interfacial slip between the tool and deformed material.

**Table IV. Size Distribution Statistics of Si Particles in FSP A356 Samples (Percent)**

| Processing Parameters | Standard Pin | | Tri-Flute Pin | |
|---|---|---|---|---|
| | <1.5 μm | >6 μm | <1.5 μm | >6 μm |
| 300 rpm–51 mm/min | 33 | 9.5 | 36 | 8.7 |
| 300 rpm–51 mm/min-T6 | — | — | 17 | 17 |
| 700 rpm–203 mm/min | 39 | 8.5 | 39 | 6.8 |
| 700 rpm–203 mm/min-T6 | — | — | 21 | 9 |
| 900 rpm–203 mm/min | 42 | 8.1 | 39 | 7.2 |
| 1100 rpm–203 mm/min | 39 | 7.0 | 40 | 6.8 |

### B. *Microstructure*

The microstructure of as-cast A356 plates was typical of unmodified sand-cast A356 with coarse needlelike Si particles and aluminum dendrites, and numerous pores. The FSP resulted in significant microstructural refinement and homogeneity, *i.e.,* significant breakup of coarse acicular Si particles and aluminum dendrites and a uniform distribution of broken Si particles in the aluminum matrix (Figures 4 through 5). The size and aspect ratio of Si particles were significantly reduced by FSP. Further, the porosity in the as-cast A356 sample was nearly eliminated by FSP (Table III).

For A356 alloy, a solid-solution treatment is usually carried out at a high temperature of ~540 °C for a long time of 8 to 16 hours to achieve complete dissolution of $Mg_2Si$ precipitates and homogenization of microstructures. The disappearance of $Mg_2Si$ phases in the FSP samples, as shown in Figure 8, indicates that all or most of the $Mg_2Si$

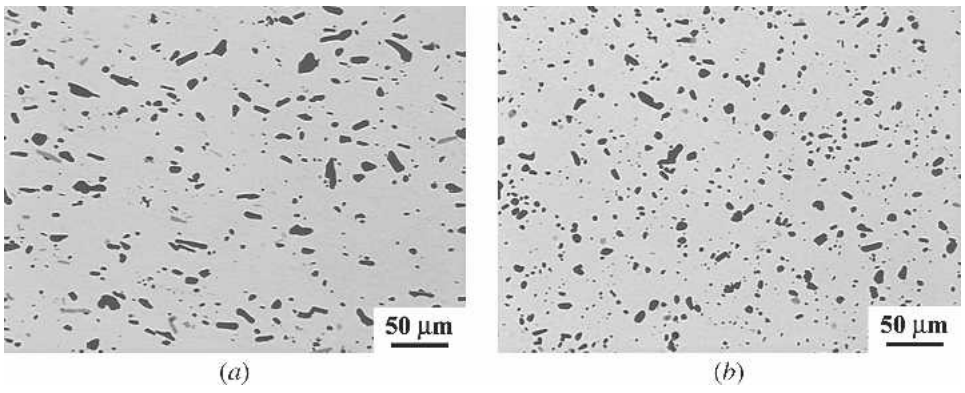


Fig. 7—Optical micrographs showing morphology and distribution of Si particles in T6-treated FSP A356 samples prepared using the triflute pin at (*a*) 300 rpm–51 mm/min and (*b*) 700 rpm–203 mm/min.

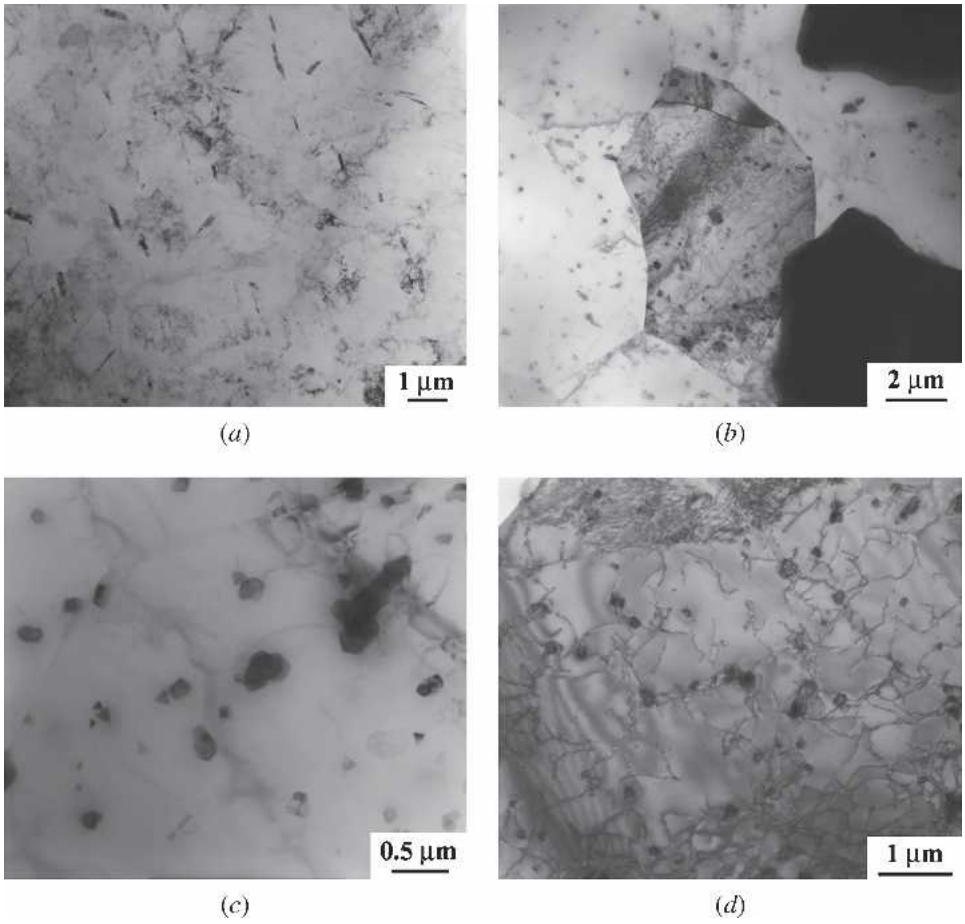


Fig. 8—TEM micrographs showing (*a*) morphology and distribution of $Mg_2Si$ precipitates in as-cast A356, (*b*) grains and fine Si particles in FSP A356, (*c*) morphology of Si particles under high magnification in FSP A356, and (*d*) interaction between fine Si particles and dislocations in FSP A356 (standard pin, 900 rpm-203 mm/min).

**Table V. Room-Temperature Tensile Properties of As-Cast and FSP A356 with and without Heat Treatment ($\dot{\varepsilon} = 10^{-3}$ s$^{-1}$)**

| | As Cast or As-FSP | | | Aged (155 °C/4 h) | | |
|---|---|---|---|---|---|---|
| Materials | UTS (MPa) | YS (MPa) | Elongation (Pct) | UTS (MPa) | YS (MPa) | Elongation (Pct) |
| As-cast | 169 ± 8 | 132 ± 3 | 3 ± 1 | 153 ± 6 | 138 ± 4 | 2 ± 1 |
| FSP, 300 rpm–51 mm/min (S-pin) | 205 ± 5 | 134 ± 4 | 31 ± 2 | 206 ± 5 | 137 ± 7 | 29 ± 2 |
| FSP, 700 rpm–203 mm/min (S-pin) | 242 ± 4 | 149 ± 7 | 31 ± 0 | 247 ± 6 | 169 ± 7 | 28 ± 1 |
| FSP, 900 rpm–203 mm/min (S-pin) | 264 ± 3 | 168 ± 9 | 31 ± 2 | 288 ± 4 | 228 ± 7 | 25 ± 2 |
| FSP, 1100 rpm–203 mm/min (S-pin) | 242 ± 3 | 157 ± 2 | 33 ± 1 | 265 ± 2 | 205 ± 5 | 23 ± 5 |
| FSP, 300 rpm–51 mm/min (T-pin) | 202 ± 4 | 137 ± 4 | 30 ± 1 | 212 ± 5 | 153 ± 16 | 26 ± 2 |
| FSP, 700 rpm–203 mm/min (T-pin) | 251 ± 4 | 171 ± 12 | 31 ± 1 | 281 ± 4 | 209 ± 2 | 26 ± 2 |
| FSP, 900 rpm–203 mm/min (T-pin) | 232 ± 3 | 140 ± 7 | 38 ± 1 | 275 ± 3 | 204 ± 5 | 30 ± 1 |
| FSP, 900 rpm–203 mm/min (T-pin)-2 pass | 255 ± 1 | 162 ± 5 | 34 ± 1 | 304 ± 3 | 236 ± 4 | 25 ± 1 |
| FSP, 1100 rpm–203 mm/min (T-pin) | 247 ± 2 | 155 ± 6 | 35 ± 1 | 256 ± 2 | 177 ± 6 | 31 ± 4 |
| FSP, 300 rpm–51 mm/min (C-pin) | 178 ± 2 | 124 ± 4 | 31 ± 3 | 175 ± 1 | 119 ± 5 | 32 ± 1 |
| FSP, 700 rpm–203 mm/min (C-pin) | 256 ± 4 | 169 ± 3 | 28 ± 1 | 264 ± 3 | 203 ± 7 | 21 ± 1 |

phases have been dissolved into aluminum matrix during the FSP thermal cycles. This is attributed to two factors. First, the maximum temperatures in the stirred region are higher than those recorded by the thermocouple (Table II), as discussed in Section A. Second, intense plastic deformation and mixing of material during FSP facilitates the dissolution of the $Mg_2Si$ phases. In this case, the dissolution of the $Mg_2Si$ phases can be completed at a lower temperature within a short time.

Figure 8 revealed the existence of numerous fine Si particles with a size of submicron or nanometer in the FSP A356. Such fine Si particles were obviously not discernable under an optical microscope. Therefore, the actual size and aspect ratio of the Si particles are lower than those

estimated by the optical microscope, as shown in Table III and Figure 6. In the as-received A356 sample, no such fine Si particles were found. The fine Si particles in the FSP A356 could have resulted from (a) an intense breaking effect of the threaded pins used in this study or (b) dissolution and precipitation of Si as secondary particles. The ultrafine Si particles in the FSP A356 samples are expected to exert a certain dispersion-strengthening effect on the aluminum matrix through the particle/dislocation interaction, as shown in Figure 8(d). This will be discussed in Section C.

Microstructural evolution and resultant mechanical properties depend on material flow characteristics during FSW/FSP. This has led to several investigations of material flow behavior during FSW/FSP in the past few years.[32–36] A number of approaches, such as the tracer technique by marker and welding of dissimilar alloys and metals, have been used to visualize material flow patterns in FSW.[32–36] In addition, some computational methods including finite element methods have been used to model the material flow.[37,38,39] However, material flow during FSW/FSP is not well understood. Reynolds *et al.*[32] and Krishnan[40] suggested that the FSW process can be roughly described as an *in-situ* extrusion process wherein the tool shoulder, the pin, the weld backing plate, and the cold base metal outside the weld zone form an ''extrusion chamber,'' which moves relative to the workpiece. During each rotation of the tool, a semicylindrical portion of the material is pushed to the back of the tool and around to the retreating side. A cross-sectional slice through such a set of semicylinders results in the onion-ring structure that is often observed in transverse sections of the FSW/FSP nugget.[40] In this case, there is very little material mixing during the FSW process. Conversely, Biallas *et al.*[41] suggested that the material flow around the pin is somewhat similar to that of regular milling of the metal. For this flow, there should be thorough mixing of material in the nugget region. The present results indicate that FSP cannot be simply considered as an extrusion process, particularly with the threaded pins used in this study. As noted earlier, FSP breaks up acicular particles into nearly equiaxed particles with sizes down to submicron, whereas an extrusion process cannot provide such breakage and distribution.

The material flow during FSW/FSP is a complicated process and depends on the tool geometry, process parameters, and material. It is proposed that the threaded pins result in a superimposed vertical and horizontal material flow from geometrical considerations. The threads tend to move material downward along the pin wall, and once this material reaches the bottom, the geometrical constraints require that the material move up and away from the pin wall. The lateral traverse of the pin requires that the material move from front to back. The interaction among these three material flow patterns, based on geometrical and volume constraints, is complex. However, significant progress has been made in understanding the complex flow patterns using marker studies coupled with computational modeling.[42] Based on intuitive considerations, higher tool rotation rate and lower traverse speed would result in more material movement and thus more mixing. Therefore, the ability of the rotating tool to break up coarse acicular Si particles and eliminate porosity increases with increasing tool rotation rate. The current study provides support to the preceding discussion. Higher tool rotation rate results in a more significant breakup of coarse acicular Si particles and aluminum dendrites and more uniform distribution of Si particles in the aluminum matrix (Figures 4 through 6 and Table III). For example, the quantity of Si particles of smaller than 1.5 $\mu$m increased from 33 pct to 39 to

**Table VI. Room-Temperature Tensile Properties of T6-treated Cast and FSP A356 ($\dot{\varepsilon} = 10^{-3}$ s$^{-1}$)**

| | T6 (540 °C/4 h + 155 °C/4 h) | | |
|---|---|---|---|
| Materials | UTS (MPa) | YS (MPa) | Elongation (Pct) |
| As cast | 220 ± 10 | 210 ± 8 | 2 ± 1 |
| FSP, 300 rpm–51 mm/min (T-pin) | 307 ± 12 | 232 ± 12 | 20 ± 1 |
| FSP, 700 rpm–203 mm/min (T-pin) | 301 ± 6 | 216 ± 11 | 28 ± 2 |
| FSP, 900 rpm–203 mm/min (T-pin) | 297 ± 8 | 213 ± 5 | 30 ± 2 |
| FSP, 900 rpm–203 mm/min (T-pin)-2 pass | 292 ± 27 | 207 ± 24 | 28 ± 9 |
| FSP, 1100 rpm–203 mm/min (T-pin) | 295 ± 6 | 212 ± 5 | 28 ± 3 |

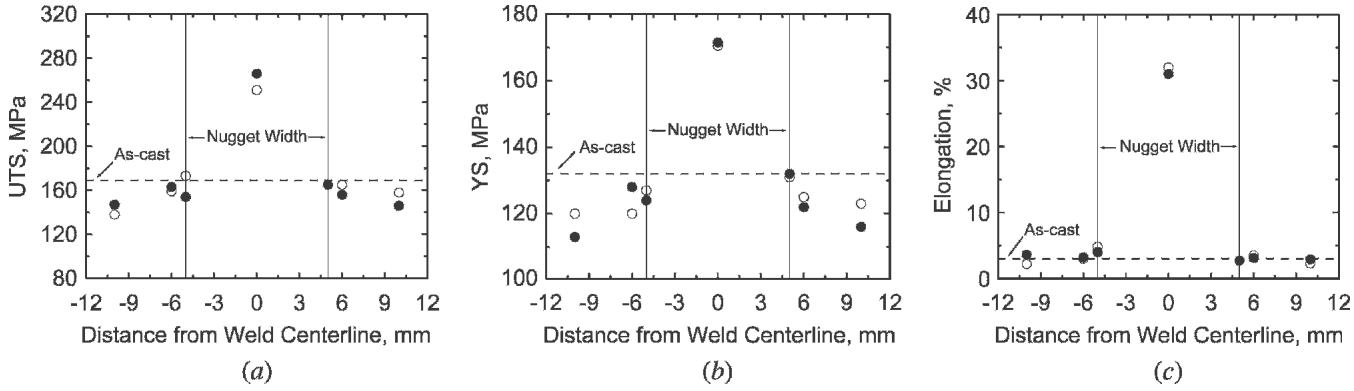


Fig. 9—Variation in tensile properties with distance from the nugget for the transition microstructure of FSP A356 (solid symbol for triflute pin, 700 rpm–203 mm/min; and open symbol for standard pin, 900 rpm–203 mm/min).

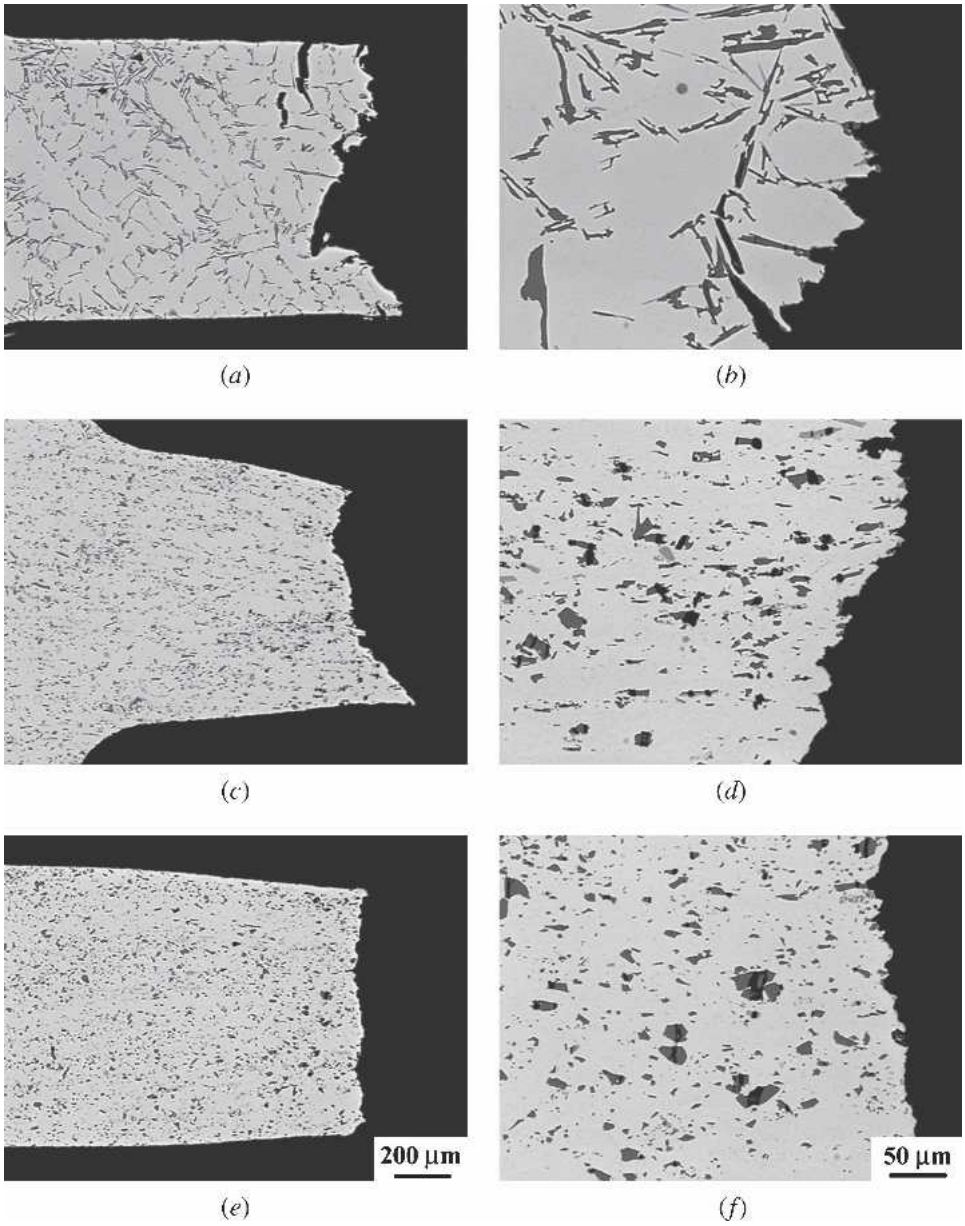


Fig. 10—Cross-sectional views of failed A356 tensile specimens: (*a*) and (*b*) as-cast; (*c*) and (*d*) as-FSP, 300 rpm–51 mm/min; and (*e*) and (*f*) as-FSP, 700 rpm–203 mm/min (triflute pin).

42 pct with increasing tool rotation rate from 300 rpm to 700 to 1100 rpm for the standard pin (Table IV).

An investigation of the effect of tool geometry on the material flow pattern and the resultant microstructure is lacking in the literature. In the present investigation, the triflute pin appears to be more effective than the standard pin and cone-shaped pin in breaking up coarse acicular particles with the investigated FSP parameter ranges (Tables III and IV). However, the understanding of the effect of tool geometry on the microstructure of FSP A356 samples is still poor.

Heat treatment at the solid solution temperature around 540 °C for long times was reported to result in a substantial degree of spheroidization and coarsening of Si particles.[8] However, the rate of spheroidization and coarsening of Si particles in unmodified A356 with coarse acicular Si particles is much lower than that in Sr- or Na-modified A356 with fine fibrous Si particles.[43,44] Therefore, no appreciable fragmentation and spheroidization of coarse acicular Si particles were observed in the present T6-treated cast A356 due to the relatively short solid solution treatment of 4 hours. Also, the T6 treatment only resulted in rounding of the sharp edges or corners of Si particles. By comparison, spheroidization and coarsening of Si particles in T6-treated FSP A356 samples were more significant than those in the cast sample due to the much smaller Si particle size in FSP samples. The coarsening is accompanied by dissolution of fine particles,[45] resulting in a significant decrease in quantity of fine Si particles in T6-treated FSP samples (Figure 7 and Table IV).

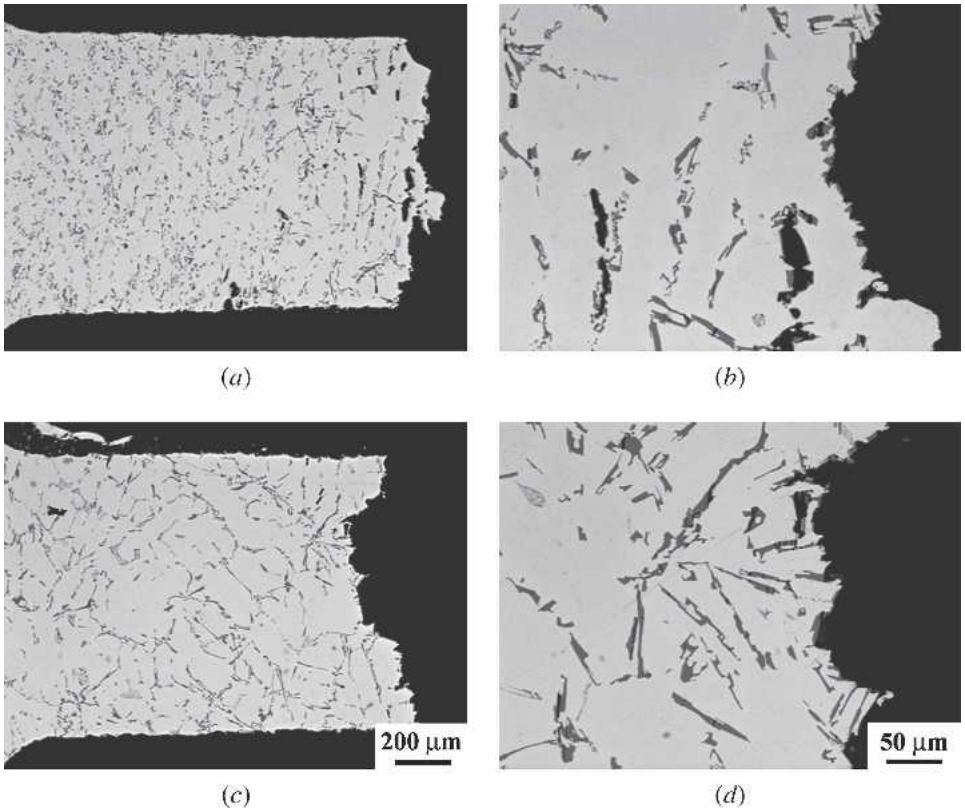


Fig. 11—Cross-sectional views of failed as-FSP A356 tensile specimens at microstructural transition regions on the retreating side: (*a*) and (*b*) transition boundary between nugget zone and parent metal and (*c*) and (*d*) 1 mm from the nugget boundary (trifluted pin, 700 rpm–203 mm/min).

### C. *Tensile Properties and Fracture Behavior*

As presented in Section B, the microstructure of the as-cast A356 consists of coarse acicular Si particles and aluminum dendrites, with casting porosity (Figure 3). Large, elongated Si particles tend to crack early during tensile deformation or interfacial separation, resulting in a reduction in both ductility and strength.[46,47,48] Furthermore, cracks also initiate at structural defects such as porosity.[49] Therefore, the present as-cast A356 sample exhibited low strength and ductility (Table V) and low strain ductile failure (Figures 10(a) and(b) and Figure 12(a)). Aging at 155 °C/4 h did not result in microstructural refinement, homogeneity, or elimination of porosity and, therefore, did not improve mechanical properties. The T6 treatment resulted in the dissolution of coarse $Mg_2Si$ in as-cast sample and the reprecipitation of fine $Mg_2Si$ and, therefore, led to an increase in strength and a reduction in ductility. However, the T6-treated cast A356 still exhibited low strain ductile failure because the T6 treatment did not lead to refinement of the coarse aluminum dendrites or acicular Si particles.

Table V shows that FSP resulted in a significant improvement in mechanical properties of A356 samples. This is attributed to remarkable microstructural refinement, homogenization, and densification, as well as precipitation strengthening resulting from FSP thermal cycles. First, breakup of coarse acicular Si particles significantly reduced Si particle cracking under low stress and consequently minimized the possibility of void initiation associated with damaged Si particles, thereby improving the ductility and increasing the strength. Furthermore, the ultrafine Si particles produced by FSP exerted an additional strengthening effect on aluminum matrix through dislocation/particle interaction, as shown in Figure 8(d). Additionally, a uniform distribution of broken Si particles also provides some improvement in strength and ductility. Second, basic elimination of porosity reduced the possibility of void initiation at such porosities, thereby improving the strength and ductility of A356 samples. Third, the microstructural refinement of aluminum matrix produced by FSP (Figure 8(b)) increased the strength of A356 samples through Hall–Petch strengthening. Fourth, all or most of the $Mg_2Si$ precipitates, the primary strengthening phase in A356, dissolved into the aluminum matrix during the FSP thermal cycle. Fast cooling from FSP temperatures retains these solutes in solution. In this case, precipitation occurred during room-temperature natural aging after FSP, resulting in an increase in the strength of the FSP samples.

Table V shows that the strength of FSP samples increased with increasing tool rotation rate from 300 to 700 rpm. This is attributed to two factors. First, the decrease in the porosity level and the decrease in the size and aspect ratio of Si particles (Tables III and IV) are beneficial for increasing strength. Second, higher tool rotation rates result in higher peak temperatures during FSP (Table II). Thus, more of the $Mg_2Si$ precipitates dissolve into the aluminum matrix during FSP at higher tool rotation rates, thereby leading to a larger precipitation strengthening effect after natural aging of the FSP samples. Above

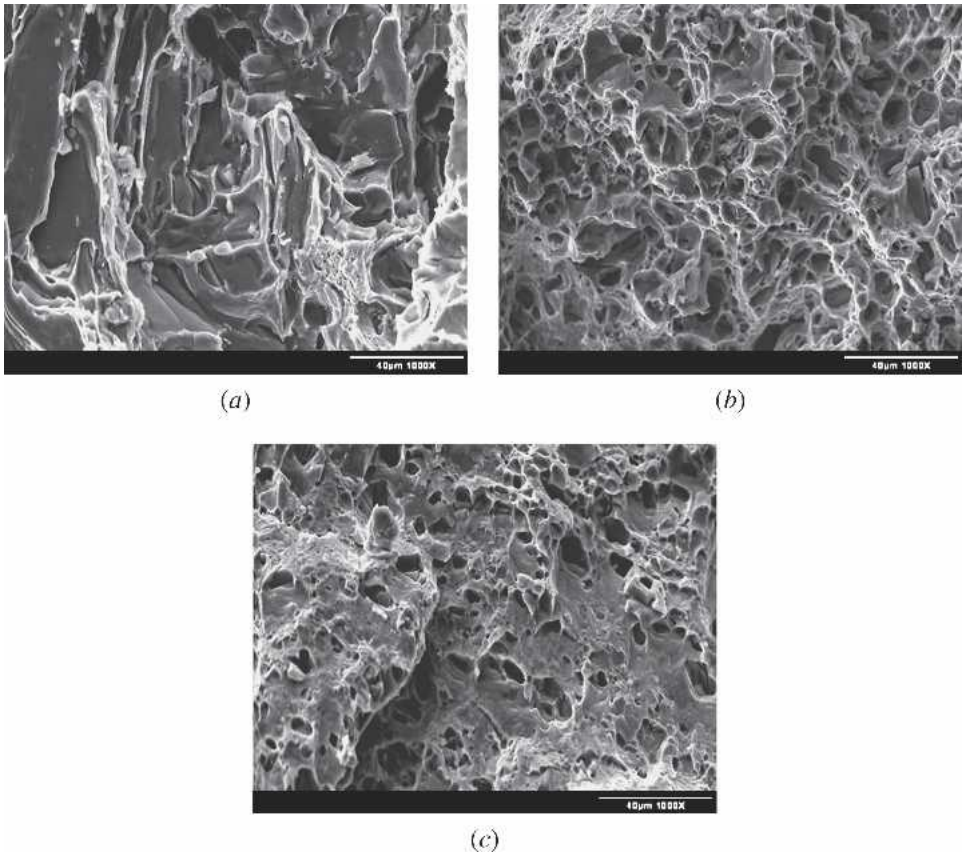


Fig. 12—SEM micrographs showing fracture surfaces of A356 tensile specimens: (*a*) as-cast; (*b*) as-FSP, 700 rpm–203 mm/min; and (*c*) FSP + T6, 700 rpm–203 mm/min (triflute pin).

700 rpm, the variation in strength of FSP A356 samples is not consistent with that of the size and aspect ratio of Si particles. However, the strength variation does appear consistent with that of the porosity level (Table III). This implies that the porosity level for FSP material is an important factor controlling the mechanical properties of A356.

Artificial aging at 155 °C for 4 hours significantly increases the strength of FSP samples prepared at the higher tool rotation rates of 700 to 1100 rpm (Table V). Again, higher tool rotation rates resulted in the dissolution of more precipitates and therefore reprecipitation during artificial aging is much more effective.

Table V shows that the two-pass FSP with 100 pct overlapping resulted in an increase in strength and a decrease in ductility. These property changes are partly attributed to a further decrease in the porosity level and the increase in the fraction of small-sized Si particles. Further, it is very likely that the two-pass processing resulted in dissolution of more precipitates with larger subsequent precipitation-strengthening during artificial aging. This is supported by the fact that aged two-pass FSP samples exhibited the highest strength among all the FSP samples.

Table V shows that the effect of tool geometry on mechanical properties is complicated and depends on the FSP parameters. For example, at 300 rpm–51 mm/min, strengths for the standard and triflute pins are higher than the cone-shaped pin, whereas at 700 rpm–203 mm/min, the cone-shaped and triflute pins are more effective in increasing the strength of A356 than the standard pin.

Table VI shows that the T6 treatment resulted in a significant increase in strength and a decrease in ductility. This is due to complete dissolution of $Mg_2Si$ precipitates during solid-solution treatment and subsequent reprecipitation during T6 aging. The precipitation-strengthening effect is similar for all T6-treated FSP A356 samples. Therefore, all T6-treated FSP samples exhibited similar strengths. The lower ductility of T6-treated FSP A356 prepared at 300 rpm–51 mm/min is attributed to a higher level of porosity. However, both FSP and cast samples exhibited similar yield strength. It is reported that changes in Si particle characteristics have little influence on the yield strength of A356, because strengthening under the T6-treatment condition is primarily achieved by $Mg_2Si$ precipitates.[48] For the FSP A356 samples, although there were numerous fine Si particles, the T6 treatment resulted in dissolution of fine Si particles, as discussed previously. Thus, the strengthening effect of $Mg_2Si$ precipitates is still dominant in the T6-treated FSP A356 samples. Therefore, T6-treated FSP A356 samples exhibited a yield strength similar to that observed in T6-treated cast A356. The increase in ultimate tensile strength of T6-treated FSP samples is mainly accounted for by the reduction in Si particle damage due to reduced particle size.

Figure 9 shows that the tensile properties of microstructural transition regions are equivalent to or lower than those of as-received parent material, and the tensile and yield strengths decrease generally with increasing distance from the FSP zone boundaries. In this transition region, FSP did not result in a significant breakup of the coarse Si particles

and aluminum dendrites, and conversely led to coarsening of precipitates. In this case, FSP did not result in an improvement in mechanical properties but actually resulted in a decrease. The control of microstructure in the transition region during FSP will be critical for achieving mechanical properties equivalent to or better than the starting material.

### D. *Practical Implications*

The overall implication of the present results is significant. These results show that FSP is a simpler and more effective microstructure modification technique for A356 castings than previous chemical and thermal treatment modification techniques. This is because FSP can simultaneously refine and homogenize the as-cast microstructure and eliminate porosity, thereby resulting in a significant improvement in tensile properties, particularly in ductility.

The FSP is a variable and flexible processing technique suitable for both localized processing for local strengthening and a large area of processing by multiple-pass FSP. Two recent investigations have demonstrated the effectiveness of multiple-pass FSP in obtaining a large area of processed region with excellent mechanical properties in cast aluminum alloys.[50,51] Single-pass FSP with a pin diameter of 8 mm usually produces a 10- to 14-mm-wide processed zone. Provided that multipass FSP is conducted with a traverse speed of 200 mm/min and a distance of 8 mm between the centers of the successive passes, it will take 25 minutes to process an area of 200 $\times$ 200 mm$^2$. Increasing the diameter of the tool pin or the traverse speed of the tool will shorten the processing time significantly. For FSW/FSP, the depth of the FSW/FSP region depends on the length of the tool pin. It has been reported that single-pass FSW can be performed to a depth of $\sim$40 mm and two-pass FSW from both sides of the plates can be used to obtain a defect-free weld of 75-mm-thick aluminum alloy plates.[52] Therefore, it is possible to modify the microstructure of aluminum plates of up to several ten millimeters thick by the FSP technique.

For Al-Si-Mg casting alloys, a T6 treatment is in most cases an essential step in the manufacturing process. Such a treatment consists of a long time solid solution heat treatment at a high temperature of around 540 °C and subsequent artificial aging at 140 °C to 170 °C.[1–13,43–49] For sand castings, the solution time is as long as 10 to 18 hours.[53] Clearly, the additional cost and production time associated with long time solid solution treatment is substantial. Furthermore, for some large components with complex shape, solution treatment and quenching are not practical. Therefore, in the past few decades, some research efforts were made to simplify the T6 treatment. The first is the so-called simplified solution treatment.[54] In this case, castings are quenched directly after the casting process and then subjected to artificial aging. However, such a simplified solution treatment does not produce maximum strengthening, because the average magnesium content in the as-cast aluminum dendrite is substantially lower than the equilibrium level.[43] The second is a short time solution treatment. Zhang *et al.*[55] reported that compared to the standard 6-hour solution treatment, 30-minute solution treatments at 540 °C to 550 °C can achieve more than 90 pct of the maximum yield strength and more than 95 pct of the maximum ultimate tensile strength and elongation to fracture. The current study shows that post-FSP aged samples prepared at the higher tool rotation rates exhibited high strength levels. For the two-pass FSP sample prepared using a triflute pin at 900 rpm–203 mm/min, post-FSP aging resulted in yield and tensile strengths equivalent or superior to those achieved by the T6 treatment. This indicates that maximum strengths can be achieved in post-FSP aged A356 samples by controlling the FSP parameters (including active cooling or heating) and tool geometry. Thus, by substituting FSP, no T6 solution treatment step is needed to achieve maximum strength. This is likely to result in a significant simplification of heat treatment and a substantial reduction in the manufacturing cost of Al-Mg-Si castings.

## V. CONCLUSIONS

1. The FSP resulted in a significant breakup of coarse acicular Si particles and primary aluminum dendrites, created a homogeneous distribution of Si particles in the aluminum matrix, and nearly eliminated all casting porosity. These microstructural modifications significantly improved the tensile properties of cast A356, in particular, ductility.
2. The tensile properties of microstructural transition regions in as-FSP samples are equivalent to or lower than those of the as-received parent material. The tensile and yield strengths decrease with increasing distance from the FSP zone boundaries.
3. Artificial aging at 155 °C for 4 hours increased both the yield and ultimate tensile strengths of FSP A356 processed at higher tool rotation rates of 700 to 1100 rpm.
4. With a T6 treatment, the ultimate tensile strength and ductility of FSP samples are significantly higher than those of cast A356. However, both FSP and cast samples exhibited similar yield strengths.
5. Two-pass FSP with 100 pct overlapping resulted in a further reduction in size and aspect ratio of Si particles and porosity level. This resulted in a substantial increase in both yield and ultimate tensile strength for both as-FSP and post-FSP aging conditions. The post-FSP aged two-pass FSP sample exhibited strengths equivalent to or superior to those of the T6-treated one-pass sample.

## ACKNOWLEDGMENTS

This work was supported by (a) the National Science Foundation, through Grant No. DMR-0076433 and the Missouri Research Board for the acquisition of a friction stir welding and processing machine, and (b) DARPA, under Contract No. MDA972-02-C-0030. One of the authors (ZYM) gratefully acknowledges the support of the National Outstanding Young Scientist Foundation with Grant No. 50525103 and the Hundred Talents Project of the Chinese Academy of Sciences.

## REFERENCES

1. D.L. Zhang and L. Zheng: *Metall. Mater. Trans. A*, 1996, vol. 27A, pp. 3983-91.
2. T. Din and J. Campbell: *Mater. Sci. Technol.*, 1996, vol. 12, pp. 644-50.

3. Y.B. Yu, P.Y. Song, S.S. Kim, and J.H. Lee: *Scripta Mater.*, 1999, vol. 41, pp. 767-71.
4. *Aluminum Casting Technology*, 2nd ed., D.L. Zalensas, ed., AFS Inc., Schaumburg, IL, 1993, p. 77.
5. S. Kumai, J. Hu, Y. Higo, and S. Nunomura: *Acta Mater.*, 1996, vol. 44, pp. 2249-57.
6. B. Zhang, D.R. Poirier, and W. Chen: *Metall. Mater. Trans. A*, 1999, vol. 30A, pp. 2659-66.
7. M.E. Seniw, J.G. Conley, and M.E. Fine: *Mater. Sci. Eng., A*, 2000, vol. A285, pp. 43-48.
8. G. Atxaga, A. Pelayo, and A.M. Irisarri: *Mater. Sci. Technol.*, 2001, vol. 17, pp. 446-50.
9. K.T. Kashyap, S. Murrall, K.S. Raman, and K.S.S. Murthy: *Mater. Sci. Technol.*, 1993, vol. 9, pp. 189-203.
10. L. Wang and S. Shivkumar: *Z. Metallkd.*, 1995, vol. 86, pp. 441-45.
11. T.J. Hurley and R.G. Atkinson: *Trans. AFS*, 1985, vol. 91, pp. 291-96.
12. D. Argo and J.E. Gruzleski: *Trans. AFS*, 1988, vol. 16, p. 65.
13. J. Wang, S. He, B. Sun, K. Li, D. Shu, and Y. Zhou: *Mater. Sci. Eng., A*, 2002, vol. A338, pp. 101-07.
14. W.M. Thomas, E.D. Nicholas, J.C. Needham, M.G. Murch, P. Templesmith, and C.J. Dawes: Great Britain Patent Application No. 9125978.8, Dec. 1991.
15. R.S. Mishra and Z.Y. Ma: *Mater. Sci. Eng., R*, 2005, vol. 50, pp. 1-78.
16. R.S. Mishra, M.W. Mahoney, S.X. McFadden, N.A. Mara, and A.K. Mukherjee: *Scripta Mater.*, 2000, vol. 42, pp. 163-68.
17. Z.Y. Ma, R.S. Mishra, and M.W. Mahoney: *Acta Mater.*, 2002, vol. 50, pp. 4419-30.
18. Z.Y. Ma and R.S. Mishra: *Acta Mater.*, 2003, vol. 51, pp. 3551-69.
19. Z.Y. Ma, R.S. Mishra, M.W. Mahoney, and R. Grimes: *Metall. Mater. Trans. A*, 2005, vol. 36A, pp. 1447-58.
20. Z.Y. Ma and R.S. Mishra: *Scripta Mater.*, 2005, vol. 53, pp. 75-80.
21. R.S. Mishra, Z.Y. Ma, and I. Charit: *Mater. Sci. Eng., A*, 2003, vol. 341A, pp. 307-10.
22. P.B. Berbon, W.H. Bingel, R.S. Mishra, C.C. Bampton, and M.W. Mahoney: *Scripta Mater.*, 2001, vol. 44, pp. 61-66.
23. J.E. Spowart, Z.Y. Ma, and R.S. Mishra: in *Friction Stir Welding and Processing II*, K.V. Jata, M.W. Mahoney, R.S. Mishra, S.L. Semiatin, and T. Lienert, eds., TMS, Warrendale, PA, 2003, pp. 243-52.
24. Z.Y. Ma, S.R. Sharma, R.S. Mishra, and M.W. Mahoney: *Mater. Sci. Forum*, 2003, vols. 426–432, pp. 2891-96.
25. S.R. Sharma, Z.Y. Ma, R.S. Mishra, and M.W. Mahoney: *Scripta Mater.*, 2004, vol. 51, pp. 237-41.
26. M.W. Mahoney, C.G. Rhodes, J.G. Flintoff, R.A. Spurling, and W.H. Bingel: *Metall. Mater. Trans. A*, 1998, vol. 29A, pp. 1955-64.
27. W. Tang, X. Guo, J.C. McClure, and L.E. Murr: *J. Mater. Processing Manufacturing Sci*, 1998, vol. 7, pp. 163-72.
28. Y.S. Sato, H. Kokawa, M. Enmoto, and S. Jogan: *Metall. Mater. Trans. A*, 1999, vol. 30A, pp. 2429-37.
29. T. Hashimoto, S. Jyogan, K. Nakata, Y.G. Kim, and M. Ushio: *Proc. 1st Int. Symp. on Friction Stir Welding*, Thousand Oaks, CA, June 14–16, 1999.
30. Y.J. Kwon, N. Saito, and I. Shigematsu: *J. Mater. Sci. Lett.*, 2002, vol. 21, pp. 1473-76.
31. Y.S. Sato, M. Urata, and H. Kokawa: *Metall. Mater. Trans. A*, 2002, vol. 33A, pp. 625-35.
32. A.P. Reynolds: *Sci. Technol. Welding Joining*, 2000, vol. 5, pp. 120-24.
33. K. Colligan: *Weld J.*, 1999, vol. 78, pp. 229S-237S.
34. B. London, M. Mahoney, W. Bingel, M. Calabrese, R.H. Bossi, and D. Waldron: in *Friction Stir Welding and Processing II*, K.V. Jata, M.W. Mahoney, R.S. Mishra, S.L. Semiatin, and T. Lienert, eds., TMS, Warrendale, PA, 2003, pp. 3–10.
35. L.E. Murr, R.D. Flores, O.V. Flores, J.C. McClure, G. Liu, and D. Brown: *Mater. Res. Innovat.*, 1998, vol. 1, pp. 211-23.
36. J.H. Ouyang and R. Kovacevic: *J. Mater. Eng. Performance*, 2002, vol. 11, pp. 51-63.
37. S. Xu, X. Deng, A.P. Reynolds, and T.U. Seidel: *Sci. Technol. Welding Joining*, 2001, vol. 6, pp. 191-93.
38. M.B. Stewart, G.P. Adamas, A.C. Nunes, Jr., and P. Romine: *Developments in Theoretical and Applied Mechanics*, Florida Atlantic University, Boca Raton, FL, 1998, pp. 472-84.
39. L. Ke, L. Xing, and J.E. Indacochea: *Joining of Advanced and Specialty Materials IV*, ASM INTERNATIONAL, Materials Park, OH, 2002, pp. 125-34.
40. K.N. Krishnan: *Mater. Sci. Eng., A*, 2002, vol. A327, pp. 246-51.
41. G. Biallas, R. Braun, C.D. Donne, G. Staniek, and W.A. Keysser: *1st Int. Conf. on Friction Stir Welds*, Thousand Oaks, CA, 1999.
42. A. Askari, S. Sillling, B. London, and M. Mahoney: in *Friction Stir Welding and Processing*, K.V. Jata, M.W. Mahoney, R.S. Mishra, and D.P. Field, eds., TMS, Warrendale, PA, 2001, pp. 43-54.
43. S. Shivkumar, S. Ricci, Jr., C. Keller, and D. Apelian: *J. Heat Treatment*, 1990, vol. 8, pp. 63-70.
44. S. Shivkumar, S. Ricci, Jr., B. Steenhoff, D. Apelian, and G. Sigworth: *AFS Trans.*, 1989, vol. 97, pp. 791-810.
45. J.W. Martin and R.D. Doherty: *Stability of Microstructure in Metallic Systems*, Cambridge University Press, Cambridge, United Kingdom, 1976, p. 35.
46. Q.C. Wang, C.H. Cáceres, and J.R. Griffiths: *ASF Trans.*, 1998, vol. 106, pp. 131-36.
47. C.H. Cáceres, C.J. Davidson, and J.R. Griffiths: *Mater. Sci. Eng., A*, 1995, vol. A197, pp. 171-79.
48. C.H. Cáceres and Q.C. Wang: *Int. J. Cast Met. Res.*, 1996, vol. 9, pp. 157-62.
49. M. Tiryakioğlu, J. Campbell, and J.T. Staley: *Scripta Mater.*, 2003, vol. 49, pp. 873-78.
50. M.L. Santella, T. Engstrom, D. Storjohann, and T.Y. Pan: *Scripta Mater.*, 2005, vol. 53, pp. 201-06.
51. Z.Y. Ma, S.R. Sharma, and R.S. Mishra: *Scripta Mater.*, 2006, vol. 54, pp. 1623-26.
52. W.M. Thomas, E.D. Nicholas, and S.D. Smith: *Aluminum 2001–Proc. TMS 2001 Aluminum Automotive and Joining Sessions*, S.K. Das, J.G. Kaufman, and T.J. Lienert, eds., TMS, Warrendale, PA, 2001, p. 213.
53. *Metals Handbook*, 9th ed., ASM, Metals Park, OH, 1988, vol. 15.
54. S. Shivkumar, S. Ricci, Jr., C. Keller, and D. Apelian: *AFS Trans.*, 1990, vol. 98, pp. 913-22.
55. D.L. Zhang, L.H. Zheng, and D.H. St John: *J. Light Met.*, 2002, vol. 2, pp. 27-36.